Supporting Information to

Nanostructured electrode enabling fast and fully-reversible MnO_2-to-Mn^{2+} conversion in mild buffered aqueous electrolytes

Mickaël Mateos [†], *Kenneth D. Harris* [‡,§], *Benoît Limoges* [†,*], *Véronique Balland* [†,*]

[†] Université de Paris, Laboratoire d'Electrochimie Moléculaire, UMR CNRS 7591, F-75013 Paris, France.

[‡] National Research Council Canada, Nanotechnology Research Centre, Edmonton, Alberta, T6G 2M9, Canada

[§] Department of Mechanical Engineering, University of Alberta, Edmonton, Alberta, T6G 2V4, Canada

* limoges@u-paris.fr, veronique.balland@u-paris.fr

I. Characterization of bare GLAD-ITO electrodes

The 1 µm-thick GLAD-ITO electrodes were characterized by cyclic voltammetry (CV) in 1 M KCl at different scan rates. The cyclic voltammograms exhibit the expected quasi-rectangular shapes for a purely capacitive behavior (Figure S1). From the linear relationship between the scan rate and the capacitive current, a capacitance of 350 µF·cm^{-2} was inferred. This value is lower than the one we previously reported for similar electrodes (*i.e.,* 530 µF·cm^{-2}).[S1] By taking into account the intrinsic capacitance of commercial 2D ITO (*i.e.*, 8 µF·cm^{-2}), an electroactive surface area enhancement of 45 was estimated for the GLAD-ITO film.

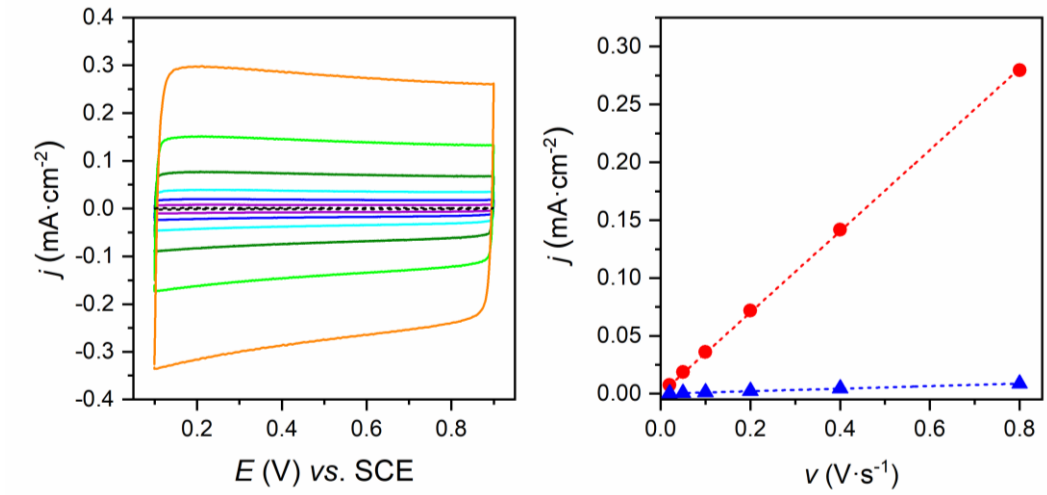

Figure S1. Cyclic voltammetry of 1 µm-Glad-ITO compared to 2D ITO in 1 M KCl. A) CV of 1µm Glad-ITO at 0.02 (purple), 0.05 (blue), 0.1 (cyan), 0.2 (olive), 0.4 (green) and 0.8 V.s^{-1}(orange) compared to 2D ITO at 0.1 V.s^{-1} (black dashed line). B) Evolution of the current density (normalized to the geometric electrode area) with the scan rate for 3D Glad ITO (red) and 2D ITO (blue).

II. Preparation and characterization of MnO_2-coated GLAD-ITO electrodes

The MnO_2-modified GLAD-ITO electrodes were prepared by potentiometric electrodeposition at a controlled anodic current (+0.3 mA·cm^{-2}) in the same electrolyte used for later galvanostatic studies, namely an acetate buffer of pH 5 along with 0.1 M $MnCl_2$ and 0.85 M KCl. The two-step procedure included a preconditioning CV (4 scans at 0.1 V s^{-1}) to improve the adhesion of MnO_2 *via* controlled nuclei formation. By simply adjusting the electrodeposition time, various thicknesses of MnO_2 deposits were obtained. The films were light to dark brown in color and homogeneous, sign of a uniform MnO_2 distribution. During MnO_2 electrodeposition, the potentiometric traces present at the very beginning (over the first few seconds) included a typical potential bump, characteristic of the nucleation and growth process occurring at the beginning of MnO_2 formation (Figure S2A). This bump is rapidly followed by a potential decrease to a constant value of 0.54 V, which remains stable for a short period. The potential then rises by 20 mV, reaching a new stable potential value (occurring at ~150 mC·cm^2 for the 1-µm-thick GLAD ITO, as illustrated by the red curve in Figure S2A). This 20 mV potential increase does not occur when MnO_2 is electrodeposited on planar ITO (black curve in Figure S2A). The onset of the potential increase is correlated with the GLAD-ITO thickness as the jump shifts to 90 and then 60 mC·cm^{-2}, when the GLAD-ITO thickness decreases to 0.6 and then 0.3 µm, respectively (orange and blue curves, Figure S2A).

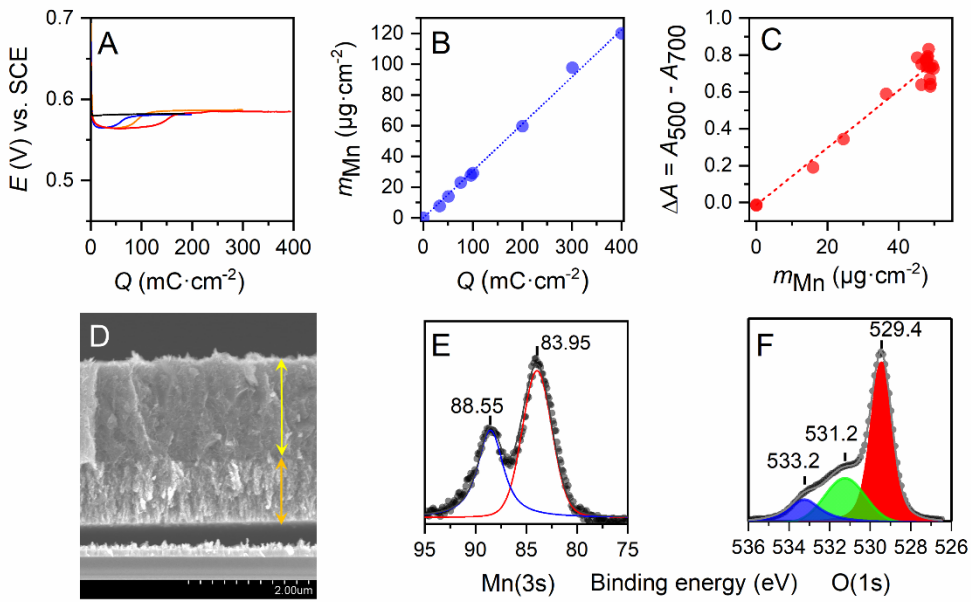

Figure S2. MnO_2-GLAD-ITO electrode characterization. A) Galvanostatic electrodeposition at 0.3 mA·cm^{-2} (preceded by a CV preconditioning step not presented) of the first MnO_2 film in 1 M acetate buffer (pH 5) containing 0.1 M $MnCl_2$. For each curve, the GLAD-ITO thicknesses were as follows: (blue) 0.3 µm, (orange) 0.6 µm, and (red) 1 µm. For comparison, the galvanostatic charging curve (in black) recorded at a planar ITO electrode under the same conditions is overlaid. (B) Amount of Mn electrodeposited on GLAD-ITO as a function of the deposited charge (determined by ICP titration and normalized to the geometric electrode area). The dashed blue line corresponds to the linear regression with a slope of 0.306 ± 0.005 µg·mC^{-1} (r^2 = 0.998). (C) Absorbance difference, *i.e.* $\Delta A = A_{500} - A_{700}$, as a function of electrodeposited mass of MnO_2 (determined by ICP). The dashed red line corresponds to the linear regression with a slope of (15.7 ± 0.1) × 10^{-3} cm^2·µg^{-1} and an intercept of -0.02 ± 0.036 (r^2 = 0.948). (D) Cross-sectional SEM image of a MnO_2 film electrodeposited over a 1-µm-thick GLAD-ITO electrode with a deposited charge of 800 mC·cm^{-2}. The orange arrow delimits the 1-µm-thick GLAD structure, while the yellow arrow delimits the MnO_2 layer that developed beyond the GLAD structure. (E) High resolution XPS spectrum of the Mn(3s) region recorded at a MnO_2-GLAD-ITO electrode (charged at 400 mC·cm^{-2}). The red and blue curves correspond to the two fitted components (ΔBE = 4.6 eV). (F) High resolution XPS spectrum of the O(1s) region. The red, blue and green curves correspond to the three fitted contributions, attributed respectively to the Mn-O-Mn, Mn-OH and H-O-H bonds.

After dissolution of the MnO_2 film in nitric acid, the amount of Mn was determined by ICP-AES, an experiment we repeated for different deposited charges (Figure S2B). The areal concentration of Mn centers (m_{Mn} in µg·cm^{-2}) linearly depends on the charge density Q (in mC·cm^{-2}) passed during the whole electrodeposition procedure. The data were modeled with a linear regression, leading to the following relationship:

$$m_{Mn} = 1000 \times \frac{M_{Mn}}{nF} \times Q = (0.306 \pm 0.005) \times Q \qquad \text{(S1)}$$

where M_{Mn} is the atomic weight of Mn (55 g·mol^{-1}), F the Faraday constant (96 485 C·mol^{-1}) and n the average number of electrons passed per deposited Mn center. Eq. S1 can be easily converted into a surface concentration of MnO_2, m_{MnO_2}, by taking into account the molecular weight of MnO_2 which leads to eq. 5 (see experimental section). Because of the low potential applied during the galvanostatic

step, we assume the faradaic contribution resulting from the oxidation of water[S2] remains negligible, leading to 100% coulombic efficiency of the MnO_2 electrodeposition. Thus, an *n* value of 1.86 can be deduced, which indicates a mix of Mn^{III} and Mn^{IV} within the electrodeposited material, as previously observed under similar experimental conditions.[S2,S3]

This *n* value is in good agreement with the average Mn oxidation state (AOS) of 3.75 estimated by XPS (eq. 7 in the experimental section) from the Mn 3s peak splitting energy (ΔBE) of 4.6 eV (Figure S1E), and which is also in agreement with that previously reported for electrodeposited MnO_2 films.[S3–S5] On the basis of the AOS of Mn and the absence of other cations in the structure, we can conclude that the chemical formula of the as-electrodeposited film is $Mn^{IV}_{0.75}Mn^{III}_{0.25}O_2H_{0.25}$. In addition, the O(1s) spectrum (Figure S2F) displays three contributions at 529.4, 531.2 and 533.2 eV, we attributed to the Mn-O-Mn, Mn-OH and H-O-H bounds, respectively.[S6,S7] The small contribution of Mn-OH compared to Mn-O-Mn corroborates the previous balance between Mn^{III} and Mn^{IV}.

The absorbance difference (ΔA), determined under open circuit potential (OCP) by subtraction of the absorbance recorded at 700 nm from that recorded at 500 nm (in order to subtract the ITO and electrolyte contributions), follows a linear relationship as a function of the amount of electrodeposited MnO_2 (m_{MnO_2}, Figure S2C). The modeling of the experimental data, arising from 20 independent electrodes, gives us the following linear relationship:

$$\Delta A_{OCP} = m_{MnO_2} \times (15.7 \pm 0.3) \times 10^{-3} - 0.02 \qquad \text{(S2)}$$

The obtained gravimetric extinction coefficient is weaker than that previously determined from thinner MnO_2 films (18.6×10^{-3} cm^2 µg^{-1} with m_{MnO_2}< 20 µg.cm^{-2}) on 2D ITO,[S3] probably because the linear approximation tends to lose its validity for high surface concentrations. Nevertheless, eq. S2 allows a rough estimate of the low surface concentrations of MnO_2 on the GLAD-ITO surface, which is typically observed at the end of a galvanostatic discharge. Thus, we are able to calculate the gravimetric capacity C_g of the MnO_2 film at the end of a galvanostatic cycling experiment (see experimental section eq. 6).

III. Electrochemical characterization of the MnO_2-GLAD-ITO electrode in a pure KCl electrolyte

The double-layer electrical capacitance of a MnO_2-GLAD-ITO electrode loaded at 100 mC·cm^{-2} was investigated in a 1 M KCl electrolyte adjusted to pH 5.0. Under these conditions, the electrode exhibits the typical features characterizing the reversible charging/discharging of an electrical double-layer, showing a linear time-dependence of charge and discharge curves with the potential (Figure S3A). The high stability absorbance switching (between 0.76 and 1.35) together with the high Coulombic efficiency of 99.1 ± 0.2 % over 400 cycles also agrees with the charging/discharging behaviour of a true capacitance (Figure S3B). From these data, a specific gravimetric capacitance of C_f = 240 ± 5 F·g^{-1} is obtained (Figure S3C), which lies in the range of capacitances commonly reported for electrodeposited MnO_2 thin-films.[S8–S12]

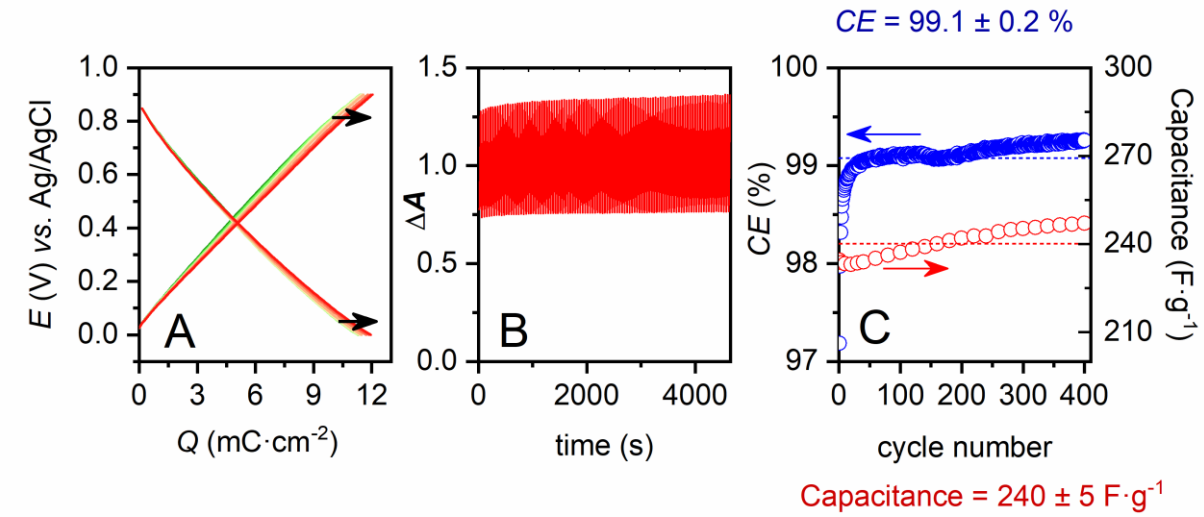

Figure S3. Galvanostatic discharging/charging experiment (400 cycles) at 0.5 mA·cm^{-2} of 1 µm-thick MnO_2-GLAD-ITO electrode in a 1 M KCl aqueous electrolyte (adjusted to pH 5), showing (A) potentiometric and B) visible absorptometric traces $\Delta A = A_{500} - A_{700}$. In (B), only the first 100 galvanostatic cycles are shown. (C) Evolution of the Coulombic efficiency and gravimetric capacitance as a function of the cycle number.

IV. MnO_2 conversion in the buffered electrolyte

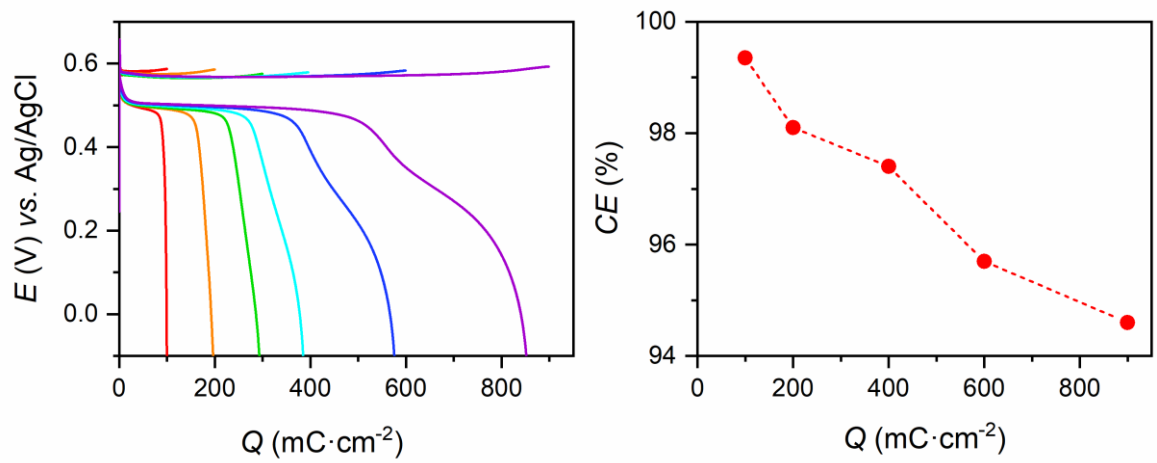

Figure S4. (A) Successive galvanostatic experiments (5 cycles) at 0.35 mA.cm^{-2} recorded at a 1-µm-thick MnO_2-GLAD-ITO electrode in a 1 M acetate buffer (pH 5) containing 0.1 $MnCl_2$ and 0.85 M KCl and for different deposited charges of MnO_2: (red) 100, (orange) 200, (green) 300, (cyan) 400, (blue) 600, and (purple) 900 mC·cm^{-2} (only the 5th cycle is represented). (B) Evolution of the Coulombic efficiency (averaged over 5 cycles) with the deposited charge.

References

(S1) Renault, C.; Andrieux, C. P. C. P.; Tucker, R. T. R. T.; Brett, M. J. M. J.; Balland, V.; Limoges, B. Unraveling the Mechanism of Catalytic Reduction of O_2 by Microperoxidase-11 Adsorbed within a Transparent 3D-Nanoporous ITO Film. *J. Am. Chem. Soc.* **2012**, *134* (15), 6834–6845. https://doi.org/10.1021/ja301193s.

(S2) Huynh, M.; Bediako, D. K.; Liu, Y.; Nocera, D. G. Nucleation and Growth Mechanisms of an Electrodeposited Manganese Oxide Oxygen Evolution Catalyst. *J. Phys. Chem. C* **2014**, *118* (30), 17142–17152. https://doi.org/10.1021/jp501768n.

(S3) Mateos, M.; Makivic, N.; Kim, Y.-S.; Limoges, B.; Balland, V. Accessing the Two-Electron Charge Storage Capacity of MnO_2 in Mild Aqueous Electrolytes. *Adv. Energy Mater.* **2020**, 2000332. https://doi.org/10.1002/aenm.202000332.

(S4) Yan, W.; Ayvazian, T.; Kim, J.; Liu, Y.; Donavan, K. C.; Xing, W.; Yang, Y.; Hemminger, J. C.; Penner, R. M. Mesoporous Manganese Oxide Nanowires for High-Capacity, High-Rate, Hybrid Electrical Energy Storage. *ACS Nano* **2011**, *5* (10), 8275–8287. https://doi.org/10.1021/nn2029583.

(S5) Chigane, M.; Ishikawa, M. Manganese Oxide Thin Film Preparation by Potentiostatic Electrolyses and Electrochromism. *J. Electrochem. Soc.* **2000**, *147* (6), 2246. https://doi.org/10.1149/1.1393515.

(S6) Chen, W.; Li, G.; Pei, A.; Li, Y.; Liao, L.; Wang, H.; Wan, J.; Liang, Z.; Chen, G.; Zhang, H.; et al. A Manganese-Hydrogen Battery with Potential for Grid-Scale Energy Storage. *Nat. Energy* **2018**, *3* (5), 428–435. https://doi.org/10.1038/s41560-018-0147-7.

(S7) Chao, D.; Zhou, W.; Ye, C.; Zhang, Q.; Chen, Y.; Gu, L.; Davey, K.; Qiao, S. Z. An Electrolytic Zn–MnO_2 Battery for High-Voltage and Scalable Energy Storage. *Angew. Chemie - Int. Ed.* **2019**, 7823–7828. https://doi.org/10.1002/anie.201904174.

(S8) Nayak, P. K.; Devaraj, S.; Munichandraiah, N. An EQCM Investigation of Electrochemical Precipitation of $Mn(OH)_2$ and Its Capacitance Behavior. *Electrochem. Solid-State Lett.* **2010**, *13* (11), 2010–2013. https://doi.org/10.1149/1.3479665.

(S9) Kuo, S. L.; Wu, N. L. Investigation of Pseudocapacitive Charge-Storage Reaction of $MnO_2 \cdot nH_2O$ Supercapacitors in Aqueous Electrolytes. *J. Electrochem. Soc.* **2006**, *153* (7), 1317–1324. https://doi.org/10.1149/1.2197667.

(S10) Castro Ruiz, C. A.; Bélanger, D.; Rochefort, D. Electrochemical and Spectroelectrochemical Evidence of Redox Transitions Involving Protons in Thin MnO2 Electrodes in Protic Ionic Liquids. *J. Phys. Chem. C* **2013**, *117* (40), 20397–20405. https://doi.org/10.1021/jp405047g.

(S11) Broughton, J. N.; Brett, M. J. Variations in MnO_2 Electrodeposition for Electrochemical Capacitors. *Electrochim. Acta* **2005**, *50* (24), 4814–4819. https://doi.org/10.1016/j.electacta.2005.03.006.

(S12) Young, M. J.; Neuber, M.; Cavanagh, A. C.; Sun, H.; Musgrave, C. B.; George, S. M. Sodium Charge Storage in Thin Films of MnO_2 Derived by Electrochemical Oxidation of MnO Atomic Layer Deposition Films. *J. Electrochem. Soc.* **2015**, *162* (14), A2753–A2761. https://doi.org/10.1149/2.0671514jes.